Dynamics of fast ions during sawtooth oscillations in the TEXTOR tokamak measured by collective Thomson scattering

S. K. Nielsen 1), M. Salewski 1), H. Bindslev 1), A. Buerger 2), V. Furtula 1), M. Kantor 2) 3) 4), S. B. Korsholm 1), H. R. Koslowski 3), A. Kramer-Flecken 3), F. Leipold 1), F. Meo 1), P. K. Michelsen 1), D. Moseev 1), J. W. Oosterbeek 3), M. Stejner 1), E. Westerhof 2) and the TEXTOR team

1) Association Euratom - Risø National Laboratory for Sustainable Energy, Technical University of Denmark, DK-4000 Roskilde, Denmark
2) FOM-Institute for Plasma Physics Rijnhuizen, Association EURATOM-FOM Trilateral Euregio Cluster, The Netherlands
3) Institute for Energy Research-Plasma Physics, Forschungszentrum Jülich GmbH, Association EURATOM-FZJ, Trilateral Euregio Cluster, 52425 Jülich, Germany
4) Ioffe Institute, RAS, Saint Petersburg 194021, Russia

e-mail contact of main author: skni@risoe.dtu.dk

Abstract. Experimental investigations of sawteeth interaction with fast ions measured by collective Thomson scattering (CTS) on TEXTOR are presented. Time-resolved measurements of localised 1D fast-ion distribution functions allow us to study fast-ion dynamics during several sawtooth cycles. Sawtooth oscillations interact strongly with the fast ion population in a wide range of plasma parameters. The phase space density for large velocities along the resolved direction oscillates out of phase with the sawtooth oscillation during hydrogen neutral beam injection. These oscillations are interpreted to originate from fast hydrogen ions with energies close to the full injection energy. At lower energies the fast ions in the plasma centre are strongly redistributed. The redistribution of fast ions from deuterium neutral beam injection in the plasma centre is dependent on the resolved direction. We find no evidence of inverted sawteeth outside the inversion radius in the fast ion distribution function.

1. Introduction

Fast-ion confinement in tokamak plasmas is essential for operation of fusion power plants. Ignition in a tokamak reactor relies on good confinement of the fusion born alpha particles which need to transfer their energy to the bulk plasma before they leave the plasma. Expulsion of fast ions from the plasma would result in a lower efficiency and may also damage the tokamak wall. A number of plasma instabilities have been found to interact with fast ions [1–4]. Amongst these instabilities is the sawtooth instability.

Sawteeth are periodic oscillations in electron pressure which occur in tokamaks when the safety factor, q, is below unity in the plasma centre [5]. In a typical sawtooth cycle the electron temperature and density, and hence the electron pressure, slowly build up and then suddenly drop at an event called the sawtooth crash. Large sawtooth crashes have been reported to trigger neoclassical tearing modes [6] which degrade the plasma confinement and may lead to a disruption of the plasma.

The trigger mechanism for the sawtooth crash is believed to be a kink mode which rapidly grows in the last few milliseconds before the crash. The kink mode is driven unstable when two conditions are fulfilled: (1) the local magnetic shear in the vicinity of the $q = 1$ surface is above a critical value, and (2) the change in ideal potential energy of the kink mode, $\delta W = \delta W_t + \delta W_f$, is below zero [7]. Here δW_t and δW_f are the bulk plasma and the fast particle contributions,

respectively. Large populations of passing fast ions are believed to prolong the sawtooth period through the δW_f term. Under many conditions the presence of fast ions in the plasma centre prolongs the sawtooth period [7–9], but it can in certain circumstances with large fractions of trapped fast ions also shorten the sawtooth period [10, 11]. A large effort has been made to control the sawtooth period by fast particles or localised current drive [6, 12, 13].
On the other hand, sawteeth are also known to react back on the fast ion population during the sawtooth collapse. Measurements done just before and just after a sawtooth collapse indicate that in some conditions the sawtooth collapse itself is associated with a reduction of the central fast ion population of up to 50% [14–18]. The sawtooth collapse is also believed to reduce the fast ion density in certain parts of phase space. The part of the fast-ion phase space density with energies below a critical energy, E_c, is reduced significantly in the plasma centre according to theory. Above E_c the reduction is highly energy and pitch angle dependent and is strongly related to the magnetic topology [19, 20].
In this article we investigate the evolution of the fast ion distribution in TEXTOR during sawtooth oscillations. The plasma is heated with neutral beam injection (NBI). We find that the phase space density of fast hydrogen ions with energies close to full beam injection energy oscillates out of phase with the sawtooth oscillation. The phase space density of these ions is almost unaffected at the time of a sawtooth crash. Contrarily, the phase space densities of ions with intermediate energies are significantly reduced over sawtooth crashes.
In section 2 we give a brief introduction to fast ion collective Thomson scattering (CTS) followed by a description of the experimental setup in section 3. Section 4 deals with the measured CTS spectra before and after a sawtooth collapse. In section 5 we describe the fast-ion development during the sawtooth cycle and at the time of the sawtooth crash. The dependence of the 1D fast ion distribution function on the radial position and on the projection direction is investigated in section 6, and finally we draw the conclusions in section 7.

2. Collective Thomson scattering

CTS is a versatile diagnostic with which several plasma parameters can be determined. CTS has previously been used to measure the ion temperature [21, 22], and the technique has also been used to obtain the 1D fast-ion velocity distribution function, $g(u)$. This was demonstrated on JET [23] where $g(u)$ was measured in a few discharges and on TEXTOR where even the time-resolved $g(u,t)$ for a wide range of plasma parameters was obtained [24–26]. Recently, results were obtained with a fast-ion CTS system on ASDEX Upgrade [27]. A CTS system for ITER is also foreseen [28–31].
CTS diagnostics use high power incident probe radiation, typically from gyrotrons, to scatter off plasma fluctuations. Part of the scattered radiation is collected by a receiver. The wave vector and the frequency of the resolved fluctuation are given by $(\mathbf{k}^\delta, \nu^\delta) = (\mathbf{k}^s - \mathbf{k}^i, \nu^s - \nu^i)$, where the superscripts i and s refer to the incident and scattered waves, respectively. When the Salpeter parameter [32], $\alpha = (k^\delta \lambda_D)^{-1}$, is above unity, the scattered radiation is dominated by the motion of the ions. Here λ_D is the Debye length. The frequency, ν^δ, of a wave vector component, $\mathbf{k}^\delta$, of the fluctuations driven by a particular ion is given by $\nu^\delta \approx \mathbf{v}_{\text{ion}} \cdot \mathbf{k}^\delta / 2\pi$. Here $\mathbf{v}_{\text{ion}}$ is the velocity of the ion setting up the fluctuation.
The measured CTS spectra are used to infer the fast-ion velocity distribution projected onto $\mathbf{k}^\delta$: $g(u) = \int d^3v\, \delta(\mathbf{k}^\delta / k^\delta \cdot \mathbf{v} - u) f(\mathbf{v})$, where $f(\mathbf{v})$ is the ion velocity distribution function in the scattering volume where probe and receiver beam patterns intersect. The CTS spectra also depend on a number of plasma parameters such as electron density, magnetic field and plasma composition which are of secondary interest in this study and are referred to as nuisance param-

eters. The parameters of interest, namely $g(u)$, are obtained by a Bayesian least square fit with nuisance parameters [33]. Most of the nuisance parameters are known from other diagnostics with a given uncertainty and contribute to the prior information. The result is then the posterior probability distribution function which is the product of the likelihood and the prior probability distribution functions.
By changing the scattering geometry, various projections of the fast-ion distribution function can be measured at various locations. By changing the resolved angle, $\phi = \angle(\mathbf{k}^{\delta}, \mathbf{B})$, and keeping the beam overlap at a similar position in the poloidal cross-section, (R, z), anisotropy in the 2D fast-ion distribution function, $f(v_{||}, v_{\perp})$, can be resolved [27]. We will demonstrate this in section 6 for the two scattering geometries shown in figure 1: both have a scattering volume located within the sawtooth inversion radius. Geometry (1) resolves the projected fast-ion distribution function nearly perpendicularly to the magnetic field ($\phi = 83°$) while geometry (2) resolves it at an angle of $\phi = 39°$.

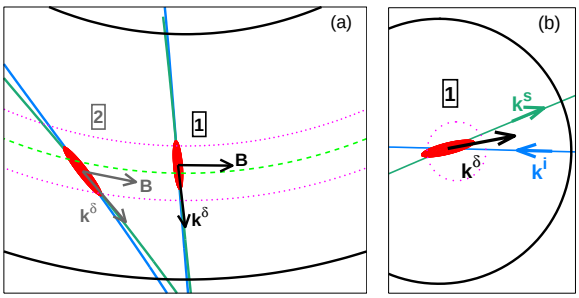

FIG. 1. Two different scattering geometries shown in top view (a) with $\phi = 83°$, $R = 1.79$ m, $z = 0.01$ m (1) and $\phi = 39°$, $R = 1.84$ m, $z = 0.02$ m (2). (Dashed line): magnetic axis, (dotted line): sawtooth inversion radius. (b): tokamak cross-section with geometry (1).

3. Experimental setup

In TEXTOR (major radius 1.75 m, minor radius 0.45 m) fast ion populations are created using two NBIs and ion cyclotron resonance heating. In the experiments reported here, we use co-current NBI with hydrogen or deuterium to heat the plasma for long sawtooth periods [34, 35]. The NBIs at TEXTOR are tangential with a tangency radius of 1.65 m such that many fast ions are born with small pitch angles in the centre. The NBI acceleration voltage is kept at 50 kV for all discharges and the injection power is typically about 1.3 MW.
The CTS diagnostic uses a gyrotron with $\nu^{i} = 109.97$ GHz and $P_i \approx 150$ kW for probing radiation [36]. The probe and receiver beam patterns are arranged such that the scattering volume has a typical radial extension $\sim$10 cm. The scattering signal is detected by a heterodyne receiver system which uses notch filters to block gyrotron stray radiation. It furthermore consists of 42 frequency channels covering the frequency range from 107 to 113 GHz with bandwidths between 80 and 750 MHz. The CTS receiver is described in details in references [37, 38] .
During CTS experiments, the magnetic field on axis is set to 2.6 T. This keeps the cold 110 GHz resonances outside the plasma. In order to separate the CTS fast-ion signal ($\sim$1-10 eV) from the background electron cyclotron emission (ECE) ($\sim$10-100 eV), the gyrotron is modulated with a 50% duty cycle with 2 ms on and 2 ms off, resulting in a time resolution of 4 ms.
An overview of the discharges considered in this article is shown in table I. First we will consider a plasma heated with hydrogen NBI. Hydrogen beam ions are accelerated to higher velocities than deuterium beam ions for a given voltage. There are therefore larger fast ion populations present in the plasma if the hydrogen NBI is used.

Shot	R (m)	ϕ (degrees)	$\overline{n}_e$ (10^{19}m^{-2})	T_{e0} (keV)	ST period (ms)	I_p (kA)	NBI
111833	1.79	110	2.7	1.8	40	440	H
106726	1.79	83	2.7	2.2	35-55	450	D
106732	1.62	83	2.6	2.1	35-50	450	D
106735	1.93	82	2.5	2.2	35-45	450	D
106737	1.84	39	2.5	2.2	40-50	450	D
106743	1.97	43	2.5	2.1	30-50	450	D

TABLE I: Overview of TEXTOR discharges presented in this article. From left: Radial position of scattering volume, resolved CTS angle, line integrated electron density, central electron temperature, sawtooth period, plasma current and NBI species.

4. Changes in spectral power density at sawtooth collapse

A theoretical spectrum for plasma parameters prior to a sawtooth collapse is shown in figure 2(a). In TEXTOR, the CTS signal with frequency shifts of a few 100 MHz from the gyrotron frequency carries information about the bulk plasma. When the frequency shift is larger than $\sim$700 MHz, the signal carries information about supra-thermal ions.

We now consider how a theoretical CTS spectrum could be expected to change over a sawtooth crash. The sawtooth crash is modeled as drops in electron density and temperature by 30% and 20%, respectively. In the model the bulk ion density is linked to the electron density via the assumption of quasi-neutrality. The other parameters are assumed constant over the crash. The plasma and geometry parameters were chosen to model discharge #111833. The result is shown in figure 2(a). The blue line represents the CTS spectrum before a sawtooth crash. The fast ion distribution has been computed with a Fokker-Planck solver assuming that hydrogen is injected into a homogeneous plasma [25]. The pitch angle and birth energy distribution (E, E/2, E/3) model the TEXTOR NBI. The green line shows the CTS spectrum after the model sawtooth crash with a reduction of the electron temperature and density only (model 1). The decrease in the electron density causes the bulk part of the spectrum to drop. The drop in electron temperature causes the width of the bulk part of the spectrum to change slightly. The black line represents a CTS spectrum with the same reductions in densities and in temperature and with additional reductions in bulk ion drift velocity by 30% and in fast ion density by 60% (model 2). The change in drift velocity causes the spectrum to shift in frequency (in this case to lower frequencies), and the reduction of the fast ion density causes the wings of the spectrum to drop. The relative differences between after and before the sawtooth crash, $(S_{post} - S_{pre})/S_{pre}$, for the two basic sawtooth models are shown in figure 2(b). The relative difference is nearly symmetric about the probe frequency if only the electron density and temperature decreases over a sawtooth crash. If also a fast ion density drop and a change in drift velocity are included, the relative difference becomes more complicated. The relative difference in the spectral power density over a sawtooth crash in discharge #111833 is overlayed in figure 2(b). The black line captures most of the trends observed in the measured data.

Sawtooth oscillations are observed in the spectral power density when the scattering volume, or a part of it, is placed within the $q = 1$ surface. The sawtooth oscillations are always present in the bulk channels. Depending on the resolved angle, the electron density and the fast ion species, the oscillations are also present in fast ion channels with different relative crash sizes. The spectral power density time traces of three representative CTS channels (out of 42) are shown in figure 3: one bulk channel at 109.51 GHz ($< \nu^i$), one bulk channel at 110.55 GHz ($> \nu^i$) and one fast-ion channel (110.95 GHz). Sawtooth signatures are evident in bulk and

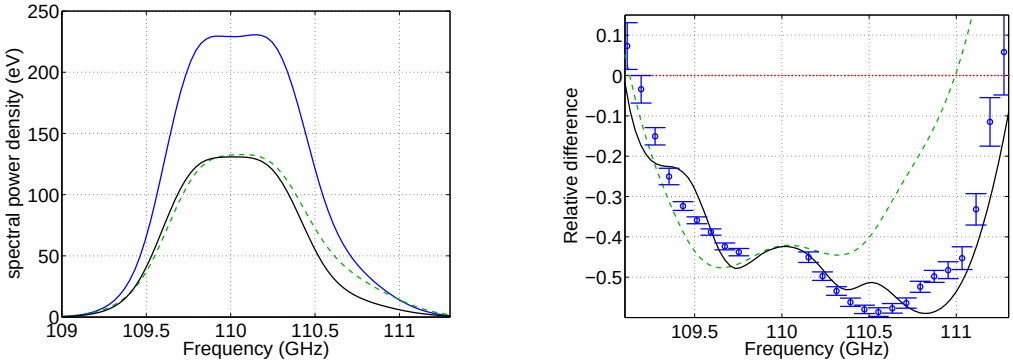

(a) Absolute spectra prior to crash (blue), after crash model 1 (green) and after crash model 2 (black).

(b) Relative crash in model 1 (Green dashed line) and model 2 (black solid line). (○): measured relative CTS signal.

FIG. 2. Absolute and relative changes in the CTS spectrum due to two sawtooth models for discharge #111833: (1) sawtooth crash reduces T_e and n_e only, (2) sawtooth crash reduces T_e, n_e, V_{drift} and N_{fast}.

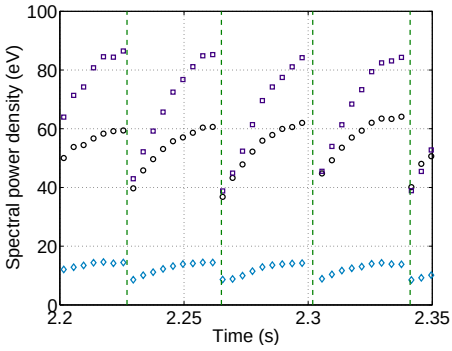

FIG. 3. Spectral power density measured with the CTS receiver in channels with center frequencies of 109.51 GHz (○), 110.55 GHz (□) and 110.95 GHz (◇). (dashed line): sawtooth crash time in T_e from ECE. (solid line): fit to measured data. Discharge #111833.

fast-ion channels.

5. Reduction of fast ion density prior to crash

In discharge 111833 the fast ion distribution was measured during a flattop co-current hydrogen NBI heating phase. The CTS geometry was such that the scattering volume was located in the plasma centre at $R = 1.79$ m with a resolved angle, ϕ, of 110°. During this phase the sawteeth in the plasma centre were reproducible with a constant period of 40 ms. The fast-ion velocity distributions were inferred from the measured spectral power densities and the given values for the nuisance parameters for this discharge. The time traces of three CTS velocity nodes are shown in figure 4(a) for $u = 1.3, 1.6$ and 1.9×10^6 m/s together with the central electron temperature. The fast-ion density with projected velocities of $u = 1.3 \times 10^6$ m/s and $u = 1.6 \times 10^6$ m/s show typical sawtooth behaviour similar to the electron temperature in the top of the graph. At the time of the sawtooth collapse these parts of the fast-ion phase space are reduced by about 40%. Nevertheless, the fast ion velocity node with $u = 1.9 \times 10^6$ m/s does not exhibit typical sawtooth behaviour. The shape of this time trace follows an oscillation which starts growing at the beginning of the sawtooth cycle, peaks half way within the sawtooth period and then gradually decreases until the time of the sawtooth collapse where the minimum is reached. This feature is magnified in figure 4(b) which is a logarithmic version of figure 4(a).

In the following we put forward a hypothesis which could explain the observed data. Figure 4 shows that a portion of the fast ion phase space density decreases before the crash. δW_f therefore drops before the sawtooth crash. If this drop is larger than any change in δW_t, this premature

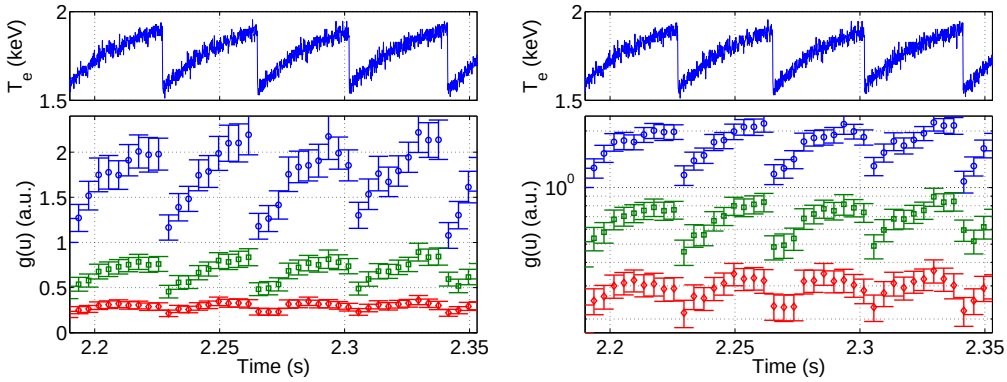

(a) linear y-scale (b) logarithmic y-scale

FIG. 4. (top): T_e from ECE, (bottom): relative fast-ion phase-space density shown for velocities (1.3(○), 1.6(□), 1.9 (◇))×10^6 m/s from top to bottom in discharge #111833. $\phi = 110°$.

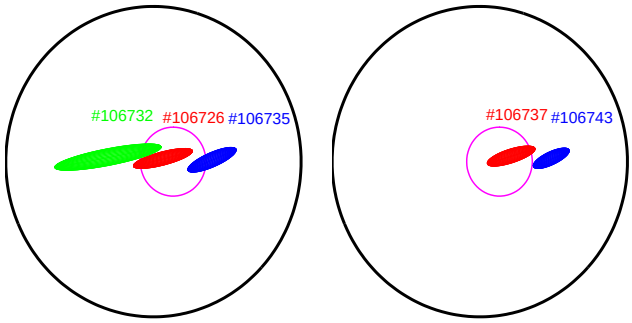

FIG. 5. CTS scattering geometries for five TEXTOR discharges. The graph to the left show geometries with $\phi \approx 80°$ *whereas* $\phi \approx 40°$ *in the right graph. The sawtooth inversion radius is represented by the magenta circle.*

disappearance of fast ions may indeed be the cause of the crash.
The sawtooth collapse itself reacts back on the fast ion population and expels fast ions with energies below a critical energy, E_c [20]. The value for E_c in this discharge is estimated from reference [20] to be in the range 50-200 keV ($3-6\times10^6$ m/s for hydrogen ions). This should be compared with the birth energies of the fast ions, E_0, $E_0/2$ and $E_0/3$, where $E_0 = 50$ keV. Thus most fast ions have energies below E_c and some fast ions might have energies close to E_c. The fastest ions with energies close to the injection energy E_0 are not reduced over the sawtooth crash ($u = 1.9\times10^6$ m/s in figure 4) which supports the theory that a critical energy exists and indicates that their energies are above the critical energy. The critical energy would then be estimated to lie below 50 keV.

6. Fast-ion dynamics dependence of position and resolved angle

A series of discharges were performed with identical plasma target parameters for a number of different CTS scattering geometries. The CTS geometries and plasma parameters are summarised in table I. The scattering volumes are visualised in figure 5. The scattering volumes shown in figure 5 (left) have a resolved angle, ϕ, close to 80° and for the geometries displayed in figure 5 (right) ϕ is around 40°. Two scattering volumes are located well within the $q = 1$ region (red). In these two discharges the resolved angles were 39° and 83°, respectively. The other three scattering volumes are located just outside, or partly within, the $q = 1$ region. The precise location of the $q = 1$ surface is not well known as no soft x-ray data is available for these discharges.

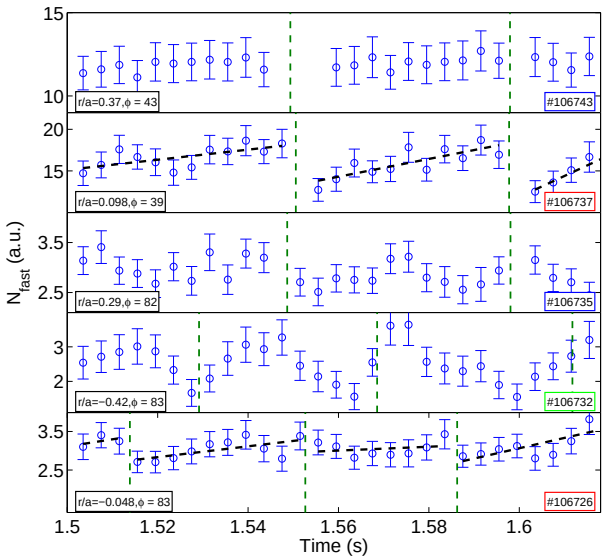

FIG. 6. Time traces of N^{-}_{fast} are shown for discharges 106726 (top), 106732, 106735, 106737 and 106743 (bottom). Fitted straight lines are included in the discharges with data from within the $q = 1$ surface.

The relative difference in the spectral power density for the discharges with the scattering located within the $q = 1$ surface (#106726, #106737) show the same features in the bulk channels as illustrated in figure 2(b). In discharge #106732 the scattering volume was partly located within the $q = 1$ surface and the relative difference in the bulk channels show similar features at a reduced level. Discharge #106735 and #106742 did not show any strong reproducible features during a sawtooth cycle.

The fast-ion velocity distributions have been obtained for these discharges. To increase the signal to noise ratio we define the *partial 1D fast-ion density* for a given resolved angle, ϕ, as $N^{-}_{fast} = \int g(u)du$ where the integration is done from $u = -2.0 \times 10^6$ m/s to $u = -1.2 \times 10^6$ m/s. The time traces of N^{-}_{fast} for the five discharges described here are presented in figure 6. The time traces for the two discharges with the scattering volume located well within the $q = 1$ surface (#106726, #106737) have been fitted with straight lines in the plot. N^{-}_{fast} does not drop strongly over sawtooth crashes in discharge #106726 ($\phi = 83°$), but it does in #106737 ($\phi = 39°$). The scattering volume is located outside the $q = 1$ surface in discharges #106732, #106735 and #106743. Here N^{-}_{fast} does not have a sawtooth structure.

7. Conclusions

We have presented measurements of the 1D fast-ion velocity distribution function, $g(u)$, at different radial locations in the plasma centre with different resolved angles. In a hydrogen NBI heated plasma, the 1D fast-ion velocity distribution decreases for velocities lower than a critical velocity at sawtooth collapses. Above this velocity, for these plasma conditions, $g(u)$ oscillates out of phase with the sawtooth cycle such that the maximum of the oscillation lies halfway through the sawtooth period and the minimum at the sawtooth collapse. This behaviour can qualitatively be explained by classical slowing down. In deuterium NBI heated plasmas, $g(u)$ shows sawtooth oscillations in the plasma centre when resolved 39° to the magnetic field whereas no strong evidence of sawtooth oscillation is found for a resolved angle of 83°. Outside the $q = 1$ surface we find no correlation between $g(u)$ and the sawtooth cycle.

Acknowledgments

This work, supported by the European Communities under the contract of Association between EURATOM and Risø DTU, FOM, and, FZJ, was carried out within the framework of the Eu-

ropean Fusion Programme. The views and opinions expressed herein do not necessarily reflect those of the European Commission.

References

[1] Heidbrink W W and Sadler G 1994 *Nucl. Fusion* **34** 535–615
[2] Pinches S D *et al.* 2004 *Plasma Phys. Control. Fusion* **46** B187–B200
[3] Rosenbluth M and Rutherford P 1975 *Phys. Rev. Lett.* **34** 1428–1431
[4] Cheng C and Chance M 1986 *Phys. Fluids* **29** 3695–3701
[5] von Goeler S, Stodiek W and Sauthoff N 1974 *Phys. Rev. Lett.* **33**(20) 1201–1203
[6] Sauter O, Westerhof E, Mayoral M L *et al.* 2002 *Phys. Rev. Lett.* **88** 105001
[7] Porcelli F, Boucher D and Rosenbluth M N 1996 *Plasma Phys. Control. Fusion* **38**(12) 2163
[8] Porcelli F 1991 *Plasma Phys. Control. Fusion* **33** 1601–1620
[9] Campbell D J *et al* 1988 *Phys. Rev. Lett.* **60** 2148–2151
[10] Graves J *et al.* 2009 *Phys. Rev. Lett.* **102** 065005
[11] Graves J P *et al.* 2010 *Phys. Plasma* **17**
[12] Hender T, Wesley J *et al.* 2007 *Nucl. Fusion* **47** S128
[13] Zohm H *et al.* 2001 *Nucl. Fusion* **41** 197
[14] Nielsen S K *et al.* 2010 *Plasma Phys. Control. Fusion* **52** 092001
[15] Marcus F B *et al.* 1991 *Plasma Phys. Control. Fusion* **33**(4) 277–287
[16] Marcus F B *et al.* 1994 *Nucl. Fusion* **34**(5) 687–701
[17] Reich M *et al.* 2007 *34th EPS conference proceedings*
[18] Kiptily V G *et al.* 2009 *Nucl. Fusion* **49** 065030
[19] Kolesnichenko Y and Yakovenko Y 1996 *Nucl. Fusion* **36** 159
[20] Kolesnichenko Y, Lutsenko V, White R and Yakovenko Y 2000 *Nucl. Fusion* **40** 1325–1341
[21] Behn R *et al.* 1989 *Physical Review Letters* **62**(24) 2833–2836
[22] Suvorov E and et al 1995 *Plasma Physics and Controlled Fusion* **37** 1207
[23] Bindslev H *et al.* 1999 *Phys. Rev. Lett.* **83**(16) 3206–3209
[24] Bindslev H *et al.* 2006 *Phys. Rev. Lett.* **97** 205005–1–2005005–4
[25] Nielsen S K *et al.* 2008 *Phys. Rev. E* **77** 016407
[26] Bindslev H *et al.* 2007 *Plasma Phys. Control. Fusion* **49** B551–B562
[27] Salewski M *et al.* 2010 *Nucl. Fusion* **50** 035012
[28] Bindslev H *et al.* 2004 *Rev. Sci. Instrum.* **75** 3598–3600
[29] Meo F *et al.* 2004 *Rev. Sci. Instrum.* **75** 3585–3588
[30] Salewski M *et al.* 2009 *Plasma Phys. Control. Fusion* **51** 035006
[31] Salewski M *et al.* 2009 *Nucl. Fusion* **49** 025006
[32] Salpeter E E 1960 *Phys. Rev.* **1**(5) 1528–1535
[33] Bindslev H 1999 *Rev. Sci. Instrum.* **70** 1093
[34] Koslowski H R 2005 *Fusion Sci. Tech.* **47**(2) 260–265
[35] Chapman I *et al.* 2008 *Nucl. Fusion* **48** 035004
[36] Woskov P *et al.* 2006 *Rev. Sci. Instrum.* **77** 10E524
[37] Korsholm S *et al.* 2006 *Rev. Sci. Instrum.* **77** 10E514
[38] Leipold F *et al.* 2008 *Rev. Sci. Instrum.* **79** 065103